RSC Advances

ROYAL SOCIETY OF CHEMISTRY

www.rsc.org/advances

Tumor specific delivery with redox-triggered mesoporous silica nanoparticles inducing neovascularization suppression and vascular normalization

Lu Sun,[a,b] Yu-Jie Liu,[a,b] Zhen-Zhen Yang,[b] Xian-Rong Qi*,[a,b,c]

a. Beijing Key Laboratory of Molecular Pharmaceutics and New Drug Delivery System, Peking University, Beijing 100191, China

b. School of Pharmaceutical Sciences, Peking University, Beijing 100191, China

c. State Key Laboratory of Natural and Biomimetic Drugs, Peking University, Beijing 100191, China

**Corresponding author. School of Pharmaceutical Sciences, Peking University, 38 Xueyuan Road, Beijing, 100191, PR China. Tel./fax: 86 10 82801584. E-mail address: qixr@bjmu.edu.cn (X.-R. Qi).*

Abstract

RNA interference (RNAi) has great potential in cancer therapy, however efficient cytoplasmic delivery still remains a major hurdle. In this study, a redox-responsive mesoporous silica nanoparticle with enlarged pores (denoted as MSN-siRNA/CrPEI) was designed by immobilizing polyethylenimine (PEI) via intermediate linkers of disulfide bond onto the MSNs as cap for redox-responsive intracellular gene delivery. The MSN-siRNA/CrPEI with high siRNA loading capacity (35 mg siRNA/g MSNs) could react to the specific reductive stimulation—upgraded glutathione concentration in tumor cells and release cargos through the rupture of disulfide bond. Subsequent, the MSN-siRNA/CrPEI was used to delivery VEGF siRNA for cancer therapy and the underlying mechanisms was explore. As we expected, the MSN-siRNA/CrPEI could be readily internalized into cells, escaped from the endolysosomes and distributed in cytoplasm where siRNA mediated its function. The MSN-siRNA/CrPEI showed remarkable anti-tumor efficacy by the suppression of neovascularization and vascular normalization after peritumoral application against mice with KB tumors, proved by interstitial fluid pressure (IFP) reduction, CD31 suppression and angioplerosis. It's noteworthy that siRNA combined with dexamethasone exerted a better treatment effect which attributed to the strong capability of dexamethasone to decrease the IFP, and a lower IFP lead to an improvement in the delivery and efficacy of exogenously administered therapeutics. These results indicate that tumor specific delivery of siRNA with redox-trigger mesoporous silica nanoparticles is a promising strategy to enhance therapeutic efficacy. Neovascularization suppression and vascular normalization may be benefits for cancer inhibition.

Keywords: mesoporous silica nanoparticle; redox-stimulation; VEGF; dexamethasone; neovascularization; vascular normalization.

Introduction

Angiogenesis is critical to the growth of human tumors and the development of metastasize[1,2]. Amongst the many proangiogenic mechanisms identified, the vascular endothelial growth factor (VEGF) signaling pathway has been implicated as the key regulator of tumor neovascularization[3]. Various therapeutic agents targeting the VEGF pathway have been successfully developed in the past decades. Bevacizumab as a humanized monoclonal VEGF specific antibody has antivascular effects in human rectal cancer[4]. Sorafenib, Sunitinib, Pazopanib, and Vandetanib as angiogenesis inhibitors not only targeting VEGF but also multiple tyrosine kinase receptors have also been approved by the Food and Drug Administration for solid tumor therapy[5, 6].

VEGF small interference RNA (siRNA) utilize the RNA interference (RNAi) to block VEGF signaling pathway in cancer therapy. It is specificity and potentness[7]. But therapeutic application of siRNA still confronts great barriers due to its instability, poor membrane permeability and short serum half-life. Currently, the promising approach widely used to initiate RNAi is delivering siRNA into the cytoplasm of target cells via delivery systems, including viral and non-viral vectors[8]. Because of the unexpected safety risks from viral vectors, non-viral delivery systems are dominated in research field, which are categorized into lipid based delivery system, polycationic polymers and inorganic nanoparticles[8]. Mesoporous silica nanoparticles (MSNs) have already been widely used as delivery systems for various active molecules. Silica materials with defined structures and surface properties are known to be biocompatible and negligible cytotoxicity[9]. Furthermore, MSNs are able to enhance the biocompatibility of several drug delivery systems, such as magnetic nanoparticles, biopolymers, and micelles[9,10]. Most of all, the high surface area, large pore volume and controllable chemistry of the MSNs allow for loading of high concentrations into the pores[11].

In many MSNs, the hexagonally symmetrical MCM-41 is one of the materials studied most commonly for drug delivery[12]. The traditional MCM-41 involving the synthesis method of liquid crystal templating has an average mesopore size of 2.5-3.7 nm[13-15] just a little bit bigger than the siRNA diameter (2.6 nm)[16], thus limiting the amount of siRNA entering into mesopores. It is also convinced that the larger pores the MSNs own, the more quantities of cargo the MSNs may load[17], the faster the MSNs may release the cargo in target cell[18], the better effect the treatment may reach, especially for siRNA which acts in a dose dependent manner that a higher siRNA concentration results in more significant inhibition of protein expression[19]. Thus, the MSNs employed here had been enlarged the mesopore through a swelling agent incorporation method.

Generally for delivery strategies, the cargo within the MSNs must be retained and doesn't release until delivery to the target cell. Therefore, the pores being "sealed" after cargo loading is required for superior MSNs. Due to the intrinsic negative charge of the silica surface via deprotonation of surface silanols, we took advantage of positively charged polymers, polyethyleneimine (PEI), which can be electrostatically attracted on MSNs' surface as supramolecular cap and retain cargo within the MSNs. PEI not only owns considerable positive charge but also possesses an intrinsic endosomal release capacity, known as the "proton sponge effect"[20]. Thus, the PEI coated MSNs can not only protect siRNA in transit from the bloodstream to the intracellular compartment, but also guarantee quick escape from the endosomal/lysosomal "pitfall", thus avoiding siRNA degradation in endosomes and lysosomes, and achieving siRNA intracellular targeting. Here, low molecular weight PEI (2 kDa) was used to coat on MSNs as cap for its lower toxicity than the long chain PEI (25 kDa)[21].

When the MSNs reach at target position, the cap on MSNs should depart after intracellular uptake and controlled release cargos. Various trigger mechanisms, such as sensitivity to pH

change, temperature, enzyme or redox condition, have been put forward[22]. The large difference in reducing potential between the intracellular and extracellular milieu enables the redox-triggered destabilization mechanism to be a promising strategy[23]. In body fluids (e.g. blood) and in extracellular matrices, a relatively high redox potential is maintained due to the low concentration of glutathione (GSH, approximately 2–20 μM). Contrary, the concentration of GSH inside cells is 0.5–10 mM, maintaining a highly reducing environment[24]. What's more, the tumor tissues own at least 4-fold higher concentrations of GSH over normal tissues, as a result the hypoxic tumor tissues are highly reducing. On account of the reducibility in the tumor intracellular milieu for the elevated GSH, the disulfide bond crosslinking is generally used[25]. Therefore, dithiobis(succinimidyl propionate) (DSP), as redox sensitive moiety, was applied to induce the thiol to construct disulfide bond so as to achieve the sensitivities to the upgraded GSH in tumor cytosol. Thus the redox-triggered MSNs possess "smart" multi-stage vesicles can stimuli sensitize according to the GSH changes in the physiological compartments, which protect siRNA from degradation and provide for timely drug release.

Based on above considerations, we report a redox-triggered MSNs (denoted as MSN-siRNA/CrPEI) in present study. The pores of MSNs were enlarged to load more siRNA. PEI of short chain was utilized as cap via disulfide linkages induced by DSP to protect the siRNA in pores (Fig. 1A). Once the siRNA loaded MSNs were internalized by tumor cells, the closed capping PEI on the surface of MSNs can be removed quickly due to the cleavage of disulfide linkages in the presence of GSH secreted by tumor cells. Subsequently, the loaded siRNA would be released from the MSNs in cytoplasm and play a role in gene silencing (Fig. 1B). As a result, a significant anti-cancer efficacy of VEGF siRNA were identified through gene silencing, tumor interstitial fluid pressure reduction, CD31 suppression, angioplerosis, and tumor shrink after peritumoral application against mice with KB tumors. In addition, the siRNA combined with dexamethasone exerted a better treatment

effect which attributed to the extraordinary ability of dexamethasone to decrease the IFP. In short, this work has demonstrated that the developed MSN-siRNA/CrPEI delivery system has great promise for delivery of siRNA in tumor therapeutics.

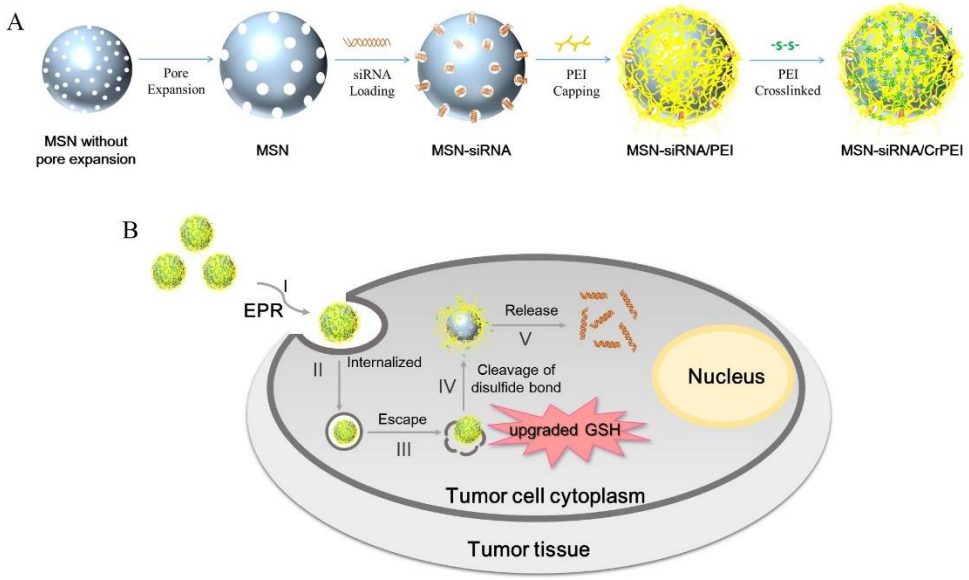

Fig. 1 (A) Scheme illustrating the preparation of MSNs as delivery vectors loading siRNA. The process includes pore expansion, encapsulating siRNA molecules into the mesopores of MSNs (MSN-siRNA), PEI-caping MSN-siRNA composite (MSN-siRNA/PEI), and crosslinking PEI via disulfide bond of DSP (MSN-siRNA/CrPEI). (B) Flowchart of tumor-triggered targeting siRNA delivery: (I) accumulation of nanoparticles via the enhanced permeability and retention (EPR) effect in tumor tissue; (II) internalization of nanoparticles into tumor cells; (III) endosomal escape of delivery vehicles; (IV) glutathione-triggred PEI loose via cleavage of disulfide bond; (V) release of siRNA into cytoplasm from the mesopores, and develop RNAi.

Material

Hexadecyltrimethylammonium bromide (CTAB) was purchased from Biofunction Co. Ltd (Beijing, China). Tetraethylorthosilicate (TEOS) was purchased from ZKTZ Chemical Technology Co .Ltd (Beijing, China). 1,3,5-trimethylbenzene (TMB) and guanidine

hydrochloride were purchased from Sinopharm Chemical Reagent Co. Ltd (Beijing, China). Branched polyethylenimine (PEI, 2 kDa) was purchased from Sigma-Aldrich (St. Louis, USA). Lomant's Reagent (DSP) was from Thermo Scientific (Waltham, MA, USA). Dithiothreitol (DTT) was purchased from Amresco (OH, USA). The scrambled siRNAs (siN.C.) and the FAM-labeled negative siRNA (FAM-siRNA) (antisense strand, 5'-ACGUGACACGUUCGGAGAATT-3'), as well as siRNA targeting VEGF (siVEGF, antisense strand, 5'-GAUCUCAUCAGGGUACUCCdTdT-3') were from Genepharma (Shanghai, China). The siRNAs are double-stranded RNA oligos containing 21 nt. All primers were synthesized by AuGCT Biotechnology (Beijing, China). Dexamethasone sodium phosphate (Dex) was purchased from Energy-chemical (Shanghai, China). RPMI-1640 medium, penicillin-streptomycin, trypsin and Hoechst 33258 were obtained from Macgene Technology (Beijing, China). LysoTracker Red was purchased from Invitrogen (Carlsbad, CA, USA). Human VEGF ELISA kit was from Raybiotech (Atlanta, Georgia, USA). Reverse Transcription System and GoTaq® qPCR Master Mix were from Promega (Madison, Wisconsin, USA). Pisum sativum agglutinin (PSA) was purchased from Vector labs (Burlingame, CA, USA).

Methods

Preparation of MSNs with enlarged pores

Synthesized silica nanoparticles were prepared according to the literature[26] with a little modification. 0.02 mmol CTAB was dissolved in 640 g methanol and 960 g water. 4.5 ml of 1 M NaOH solution together with 4 ml of TEOS were added to the solution with vigorous stirring for 8 h followed by the mixture being placed overnight to obtain white precipitate, which was centrifugated and washed with ethanol and water three times each to remove remaining surfactant. Then the synthesized silica nanoparticles were dispersed in ethanol and

sonicated for 30 min. 25 ml of 1:1 mixture (v/v) of water and TMB was added subsequently to prepare the silica nanoparticles with enlarged pores. The mixture was placed in the pressure reactor with thick wall and kept stewing at 140°C for 4 days.

The obtained powder was washed with ethanol and water five times each, and refluxed in 200 ml acidic ethanolic solution (100 ml ethanol added with 1 ml concentrated hydrochloric acid) overnight. Afterwards the white product was filtered out, washed with ethanol and then dried up in vacuum oven for 12 h.

Preparation of MSN-siRNA/CrPEI

The encapsulation of siRNA into MSNs was carried out in dehydration condition[15]. In brief, 0.3 mg synthesized MSNs were dispersed in 100 μl ethanol by probe supersonic, followed by adding 10 μl 12 M guanidine hydrochloride salt (Guan-HCl) and 20 μl water solution of siRNA. The mixture was dispersed by vortex for 30 s and then was shaken with 100 rpm at 25°C for 1 h continuously. The amount of adsorbed siRNA was determined from the different concentration of siRNA in solutions before and after adsorption process by Nanodrop 2000 spectrophotometer (Thermo Scientific, USA).

Then the siRNA-loaded MSNs (MSN-siRNA) were dispersed in PEI ethanol solution to acquire aggregates capped with PEI (MSN-siRNA/PEI). After vortex for 30 s, the mixture was incubated at 25°C for 20 min, then centrifuged at 5000 rpm for 10 min to remove the free PEI in supernatant. The determination of PEI concentration in ethanol solution was using the standard curve plotted by measuring the absorption value at 220 nm through TU-1900 spectrophotometer. The amount of capped PEI could be calculated from the different concentration of PEI in solutions before and after PEI-capping process.

To achieve PEI crosslinked by disulfide bond, 0.01 M DSP in dimethylsulfoxide (DMSO) was added to the preformed aggregates dispersed in ethanol[27]. The solutions were mixed by

vigorous vortex and incubated at 25°C for 30 min. Then the obtained MSN-siRNA/CrPEI aggregates were promoted the dispersion by being incubated in acidic deionized water under sonication for several minutes. The aggregates were later treated with deionized water to get the MSN-siRNA/CrPEI complex.

Characterizations of MSNs

Nitrogen adsorption-desorption isotherms were measured at 77 K with 100 mg of MSNs, using an Accelerated Surface Area and Porosimetry System (ASAP 2020). Before the measurements, all samples were degassed at 300°C for 12 h. Surface area calculations were carried out via the Brunauer-Emmett-Teller (BET) multimolecular layer adsorption model. Whereas the average pore sizes were calculated from the desorption branch by using the Barrett-Joyner-Halenda (BJH) model.

Transmission electron microscope (TEM) observation was carried out on a JEM-2100F transmission electron microscope. Samples were prepared in ethanol, and a drop of each suspension was placed onto the copper grid. The grids were then dried at room temperature for several hours before TEM observation.

The zeta potentials were measured via the Malvern Zetasizer Nano ZS (Malvern, UK) in automatic measurement position and laser attenuation.

In vitro release experiments

The PEI capping function were investigated by the release profiles of siRNA from the obtained MSN-siRNA/CrPEI. The release profiles of siRNA with and without dithiothreitol (DTT) at pH 7.4 were carried out as follows. Two parallel vials contain MSN-siRNA/CrPEI (2.0 mg) had been dispersed in 2.0 ml phosphate buffer (PBS) with pH 7.4 at 37°C. After 16 h, 2 ml of 10 μM DTT solution was added in one MSN-siRNA/CrPEI vials. At particular

time intervals, 10 μl of sample from dissolution medium was collected and the same volume of fresh solution was added. After centrifugation at 12,000 rpm for 3 min, the supernatant of samples were analyzed by Nanodrop 2000 (Thermo Scientific, USA). Each assay was repeated in triplicates. The siRNA release from MSN-siRNA/PEI was also carried out as comparison.

Cell culture

KB cells were grown in RPMI-1640 medium supplemented with 10% fetal bovine serum (FBS, Sijiqing, China), 100 IU/ml penicillin and 100 mg/ml streptomycin. All cells were maintained in a 37°C humidified incubator with a 5% CO_2 atmosphere.

Cellular uptake

The cellular uptake of the nanoparticles loaded with FAM-siRNA was confirmed by fluorescence detection. KB cells were seeded in six-well plates at a density of 5×10^5 cells per well in 2 ml of complete 1640 medium for 24 h. The cells were rinsed with PBS and incubated with MSN-siRNA/PEI and MSN-siRNA/CrPEI containing FAM-siRNA (50 nM) in serum-free medium. After incubation for 4 h at 37°C, the cells were rinsed with cold PBS, trypsinized and washed three times with cold PBS containing heparin (125 U/ml). The samples were centrifuged, resuspended and determined immediately by flow cytometry.

Intracellular trafficking and endosomal escape

A confocal fluorescent microscope was used to compare the intracellular distribution of the nanoparticles. KB cells were seeded on glass-bottom dishes at a density of 2.5×10^5 per well containing complete 1640 medium for 24 h. After three washes with PBS, the nanoparticles were treated in serum-free medium for 4 h at 37°C. The final concentrations of FAM-siRNA

in the culture medium were 50 nM. Subsequently, the cells were rinsed with cold PBS containing heparin (125 U/ml) three times and fixed with 4% formaldehyde for 15 min at room temperature. Following another three rinses with cold PBS, the cell nuclei were stained with Hoechst 33258 (5 mg/ml) for 20 min at 37°C. Then the cells were imaged using a confocal laser scanning microscope (CLSM, Leica, Heidelberg, Germany). FAM-siRNA and Hoechst 33258 were excited using 488 nm and 345 nm lasers, respectively.

To track the internalization and endosomal escape of FAM-siRNA, KB cells were incubated for 0.5 h, 1 h, 2 h, 3 h, and 4 h with MSN-siRNA/CrPEI. Then, endosome/lysosome labeling was performed by LysoTracker Red (250 nM) for 30 min. After nuclear staining, the cells were observed by a CLSM. The LysoTracker Red was excited by 561 nm lasers.

Cytotoxicity evaluation

The cytotoxicity of the nanoparticles (MSN/CrPEI) was evaluated via MTT assay. KB cells were seeded on 96-well plates at the density of 1×10^5 cells per well in 180 μl complete 1640 medium for 24 h. Then cells were exposed to fresh culture medium containing MSN/CrPEI of different concentrations ranging from 10 μg/ml to 100 μg/ml for additional 48 h, followed by staining with MTT (5 μg/ml). After 4 h of incubation at 37°C, the growth medium was replaced with 200 μl DMSO. Absorbance was measured at 570 nm through an iMark™ microplate absorbance reader (Bio-Rad, USA).

In vitro siRNA transfection and gene expression

In vitro RNAi experiment was carried out according to our previously literature[19]. For VEGF protein assessment, KB cells were seeded into six-well plates at a density of 2×10^5 per well. The amount of silencing VEGF in the supernatant medium was quantified by a human

VEGF immunoassay kit (RayBiotech, USA) according to the instructions of manufacturer. The total protein concentration was determined using a BCA Protein Assay Kit. For the cellular level of VEGF mRNA, quantitative real-time polymerase chain reaction (qRT-PCR) method was applied. KB cells were seeded into 25 cm^2 culture flasks at a density of 1×10^6 per well for 24 h. The final concentration of siRNA (VEGF siRNA or siN.C.) employed in the experiment was 80 nM. All experiments were performed in triplicate.

In vivo tumor growth inhibition and body weight change

The anti-tumor efficacy was investigated using the xenograft tumor model. All animal procedures were performed with the approval of the Institutional Animal Care and Use Committee at Peking University Health Science Center. Female BALB/c nude mice (16 ± 2 g) were purchased from Vital River (Beijing, China), and kept in standard housing conditions with free access to standard food and water. KB cells (5.0×10^6) were implanted subcutaneously in the right armpit of nude mice. When the tumor volume reached approximately 100 mm^3, the mice were randomly divided into two groups (n=5 per group) and treated with 50 μl of 5% glucose (control) and MSN-siRNA/CrPEI via peritumoral injection, respectively. The doses of VEGF siRNA was 1.0 mg/kg. Injection was performed every two days and total three times. The anti-tumor effect was evaluated in term of the tumor volume which was calculated by the formula: Volume (mm^3) = $a\times b^2/2$, where a and b are the major axis and minor axis of the tumor, respectively, as reported previously [28]. After 6 days, the mice were sacrificed and the tumors were harvested, weighed and photographed. The body weight of each mouse was monitored every day.

Interstitial fluid pressure

Interstitial fluid pressure (IFP) in the KB tumors was measured using an established

wick-in-needle technique before tumor resection[29]. Four nude mice per group were anesthetized by sodium pentobarbital solution and 2 to 3 measurements per tumor were made. IFP was recorded and calculated as the pressure change from baseline to average maximum pressure measured more than 10 seconds[30].

Perfusion and microvessel density observation

The perfusion analysis was carried out by referring to the literature[30]. Three nude mice bearing tumors per group were received an intravenous injection of fluorescence-pisumsativum agglutinin (PSA). One hour later, the mice were euthanized. Tumor sections were frozen and cut into 4 μm thick sections. All frozen sections were analyzed using CLSM.

To observe intratumoral microvessel density, the frozen sections of harvested tumors were fixed in 4% paraformaldehyde. After blocked with goat serum (10% in PBS), sections were further treated with CD31 antibody (Abcam, UK) followed by fluorescent secondary antibody and Hoechst 33258. All frozen sections stained with CD31 were analyzed using CLSM.

Determination of intratumoral VEGF contents

To determine the intratumor VEGF expression, approximately 100 mg tumor tissues were treated for total protein and mRNA extraction followed by ELISA and qRT-PCR assay, respectively. Tumor tissues were homogenized and incubate with 600 μl RIPA tissue lysis buffer (1% 100 mM PMSF), and then centrifuged for 10 min at 12,000 rpm. The total protein and VEGF protein concentration were determined by a BCA Protein Assay Kit and human VEGF immunoassay kit (RayBiotech, USA), respectively. To evaluate the levels of VEGF mRNA, each extracted mRNA samples were normalized to the same 260 nm absorbance

value and detected via qRT-PCR as described above.

Dexamethasone administration

After the tumor volume reached approximately 100 mm^3, dexamethasone (Dex) was administrated intravenously on day 1, 2, 3 and 5, meanwhile siRNA-loaded formulation was administrated peritumoral on day 3, 5 and 7. The dose of siRNA and dexamethasone was 1.00 mg/kg and 3 mg/kg, respectively. After 8 days, the mice were sacrificed and the tumors were harvested, weighed and photographed. The tumor volume, IFP, blood perfusion, microvessel density, intratumoral VEGF contents and the body weight was evaluated as describe above.

Statistical analysis

All data was analyzed using student's t-test in statistical evaluation. P value <0.05 was considered to indicate statistically significance (*P<0.05, **P<0.01).

Results and Discussion

Characterizations of MSNs

MSNs with homogeneous size and morphology were prepared by TEOS as a silica source and cationic surfactant CTAB as a structure directing agent. Then the MSNs possessed enlarged pores with TMB as a hydrophobic swelling agent. TMB has a suitable size, which make it possible to penetrate into micelle rod inside mesopores driven by the hydrophobic forces between surfactant alkyl chain and TMB, thus enlarging the hydrophobic core of micelle and the pores, while retaining the morphology, monodispersity mesopores[14]. The finally synthesized MSNs had an average particle diameter around 160 nm (Fig. 2A), BET surface areas 771.65 m^2/g, BJH pore sizes around 5.7 nm (Fig. 2B), pore volumes 1.67 cm^3/g (Fig. 2C) much bigger than the traditional type of MCM-41, which has pore sizes around 2.7

nm, pore volumes 1 cm^3/g[14]. Fig. 2D showed the nitrogen sorption isotherm. At a relative pressure of $0.6<P/P_0<0.8$, a steep increase occurred and a desorption hysteresis loop appeared, which is a type IV for H1 hysteresis loop classified by IUPAC, that indicates the material has the ordered mesopore[31].

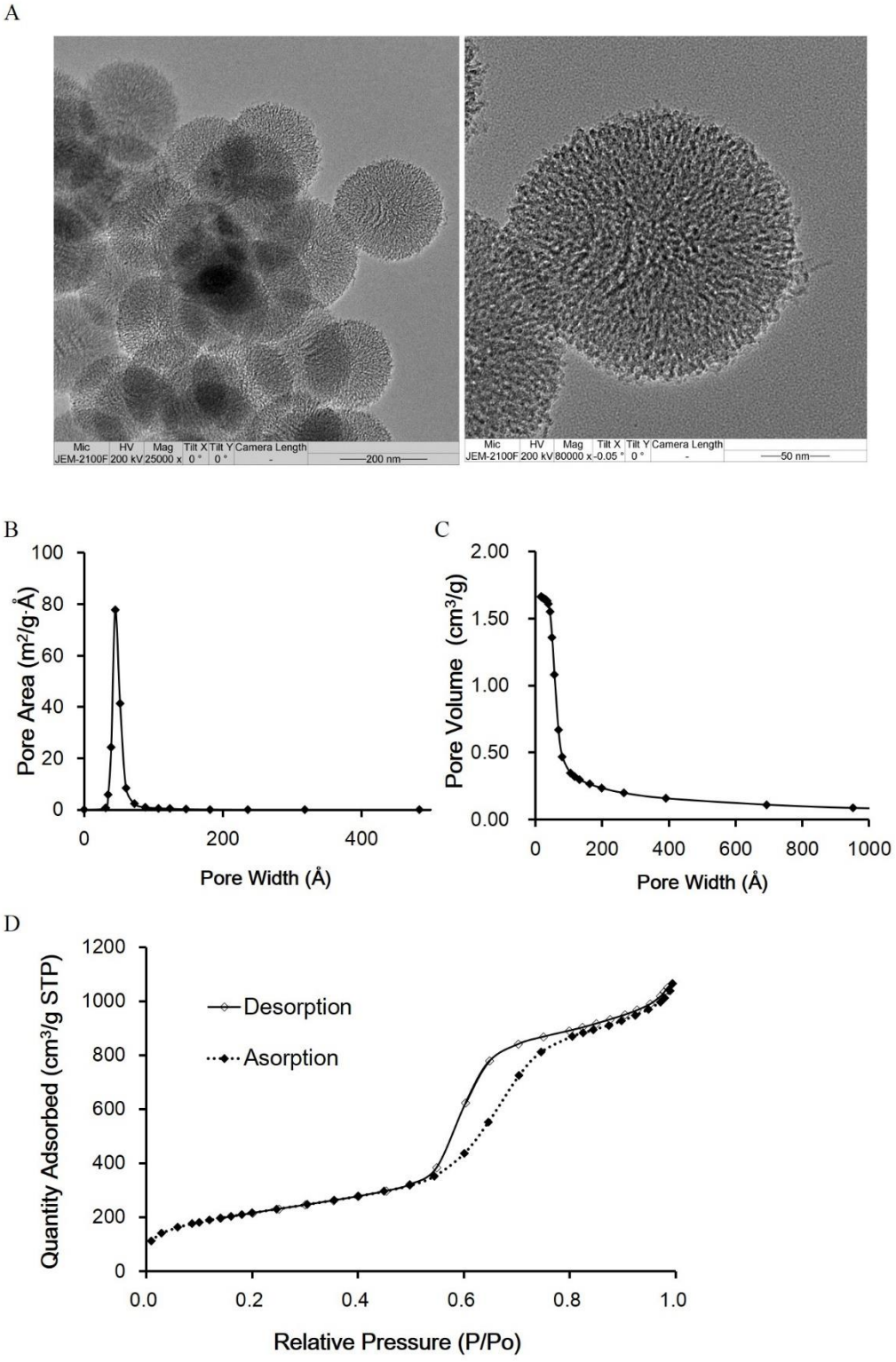

Fig. 2 Characterizations of MSNs. (A) TEM for MSNs; (B) BJH desorption dA/dw pore area; (C) BJH desorption cumulative pore volume; (D) Nitrogen adsorption-desorption isotherms.

Characterizations of MSN-siRNA/CrPEI

In hydrophilic solution, both siRNA and MSNs surfaces are negative and mutual repulsion. However, previous literature reported that the high concentration of ions in the chaotropic salt solution could decrease Debye Length and shields the negative charges so as to weaken the repulsive electrostatic force between siRNA and MSN[15]. Here, we utilized the published method with a little modification that 0.923 M Guan-HCl and 76.9% ethanol (v/v) as the composition of chaotropic salt solution was taken advantage. It is reported that Guan-HCl possess the outstanding ability to catch water molecules, thus offering the shielded intermolecular electrostatic force, dehydration effect, and intermolecular hydrogen bonds to facilitate siRNA's diffusion into the mesoporous structure, while organic solvent induce the dehydrated effect to ensure siRNA to be encapsulated within MSN mesopores[32]. The loading efficiency of siRNA was about 65%, and the amount of siRNA-loaded by MSNs could reach 35 mg/g on average which is higher than that of traditional loading of MSNs (27 mg siRNA/g MSNs)[33]. The higher loading capacity may result from the enlarged pores.

To prepare PEI-coating MSNs, the siRNA-loaded MSNs were mixed with PEI in ethanol solution. Because siRNA was insoluble in ethanol, PEI solution was enough hydrophobicity that adsorbed siRNA would not desorpt from the pores[15]. The amount of PEI coating on MSNs is 70 μg/mg, which was calculated from the differences of PEI concentration in solutions before and after PEI-coating process via the standard curve of PEI concentration in ethanol.

The MSNs coated with PEI were subsequently crosslinked by the addition of the appropriate amount of DSP solution to introduce the disulfide bond by only one step reaction

to turn the nanoparticle stable. The molar ratio of DSP and PEI was 2. Based on the calculated amount of PEI, the number of DSP we needed was 8.10×10^{-8} mol/g MSNs.

Every process of mesoporous silica was characterized by TEM. Fig. 3 showed the TEM micrographs of such vehicle with different process respectively. Compared to naked or bare MSNs (Fig. 3A), the mesoporous structure of MSN-siRNA (Fig. 3B), MSN-siRNA/PEI (Fig. 3C), and MSN-siRNA/CrPEI (Fig. 3D) became fuzzy gradually and the size of nanoparticles changed from 175 nm (bare MSNs) to 210 nm (MSN-siRNA/CrPEI), which also confirmed that the MSNs had been loaded with siRNA and embedded within the PEI layer and had a crosslinked PEI layer successfully. The thick of PEI layer was about 15 nm.

The bare MSNs displayed negative zeta potential (–(26.9 ±1.05) mV, Fig. 3E). The positive zeta potential of MSN-siRNA/PEI (+ (16.9 ±0.30) mV) was provided by PEI for its abundant primary amines. In addition, the zeta potential of MSN-siRNA/CrPEI (+(1.82 ±1.08) mV) was much smaller than that of MSN-siRNA/PEI, indicating the crosslinking of PEI via disulfide bond resulted in many amide bonds that contributed to an acute reduction of protonable primary amines of PEI, which may also decrease the toxicity from PEI on cells.

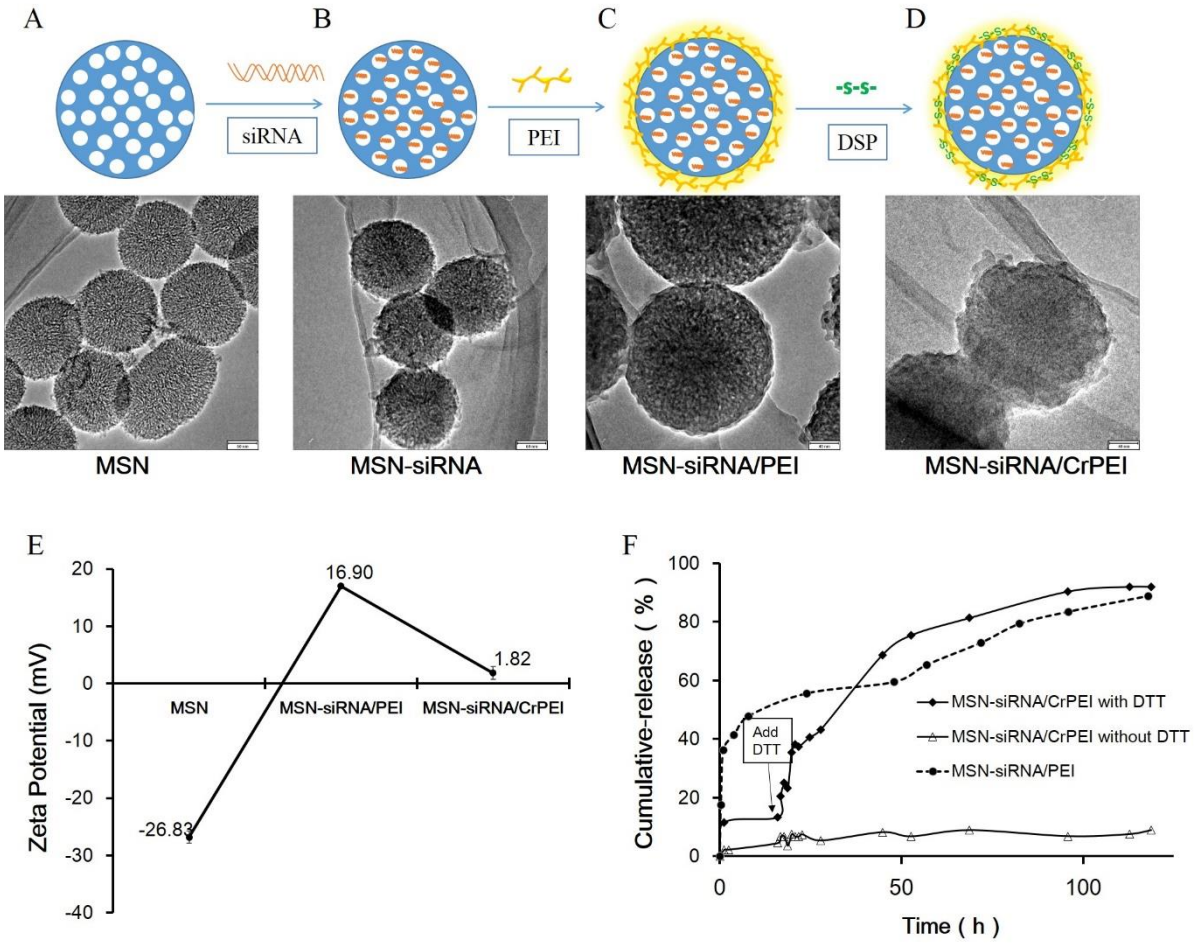

Fig. 3 Characterizations of MSN-siRNA/CrPEI. TEM of (A) bare MSNs, (B) MSNs loaded with siRNA in the mesopores, (C) PEI capped MSN-siRNA, and (D) disulfide bond crosslinked PEI capped MSN-siRNA. The scale bar in A and B is 60 nm, and in C and D is 40 nm. (E) Zeta potential of various MSNs. (F) siRNA release profiles of MSN-siRNA/CrPEI and MSN-siRNA/PEI in phosphate buffer solution (PBS) at pH 7.4.

siRNA release

In order to evaluate the crosslinked PEI via disulfide linkages having sensibility to reductive environment or not, DTT, a small reductive molecule used to simulate the effect of GSH, was added to investigate the siRNA release in vitro. As shown in Fig. 3F, there was no siRNA could be detected during 120 h in the absence of DTT, indicating the efficient confinement of siRNA in the mesopore of MSNs capped with PEI. In contrast, there was a

burst release of siRNA with the addition of DTT due to the cleavage of disulfide bond. In reductive condition, the cumulative drug release percentage was about ~90% at pH 7.4 after 120 h release. Whereas for MSN-siRNA/PEI, the burst release of siRNA was observed during the first hour, suggesting the short chain PEI desorpted from the surface of MSNs and released siRNA in aquatic environment.

In our study, we took advantage of short chain PEI (2 kD) that owned less amino groups and positive charge than the long chain PEI (25 kD), thus making it more easier to fall off from the MSNs surface, which would cause siRNA release. The results suggest that the MSNs could be an effective siRNA carrier and encapsulate siRNA without release until the cap on MSNs was removed by the cleavage of disulfide bond induced by DTT or GSH in cells. This redox-triggered destabilization mechanism is the outcome of large differences in the GSH concentration found in different tissues. In the circulation of the blood, there is not enough reductant to cleavage the disulfide bond (the intracellular GSH level in normal tissue is 1-10 mM, but that in the blood is 2 μM). While in tumor tissue environment, where GSH concentration is 7 to 10 times higher than that in normal cells[34]. Thus, the nanoparticles were internalized into the tumor cells that offered a higher GSH level than extracellular environment. As a consequence, it is much easier for the extremely elevated GSHs to split the crosslinked PEI cap and release the cargo.

In briefly, the prepared MSN-siRNA/CrPEI possess high loading of siRNA and can stimuli sensitize according to the GSH changes in the physiological compartments, which is “smart” multi-stage vesicles, protect siRNA from degradation in circulation and provide for timely drug release in tumor cells. In addition, the nature of the MSN-siRNA/CrPEI is intended to bestow drug carriers with suitable properties for passive localization in tumor tissues by the EPR effect[35]. All these features suggested applications for drug delivery in specific biological compartments.

Cellular uptake, intracellular trafficking and endosomal escape

Poor membrane permeability of siRNA with the large MW (about 13.3 kDa) and hydrophilic nature makes the therapeutic application a difficulty[7]. Two spectroscopy techniques were used to determine the cellular uptake, including flow cytometry and confocal fluorescent microscopy. Free FAM-siRNA and FAM-siRNA-loaded MSNs (MSN-siRNA/CrPEI and MSN-siRNA/PEI) that the siRNA concentration was 50 nM, together with KB cells were incubated for 4 hours at 37°C. The result of flow cytometry was indicated in Fig. 4A. Naked siRNA showed low florescence intensity, indicating little translocation of siRNA into cells, which was consistent with the nature that was poor membrane permeability of naked siRNA. Both MSN-siRNA/CrPEI and MSN-siRNA/PEI presented significant uptake than that of control and naked siRNA. Furthermore, MSN-siRNA/CrPEI performed a little bit higher uptake of FAM-siRNA than that of merely capped with PEI, suggesting more translocation of siRNA into the cells. This is perhaps the processes that when electropositive PEI combined with electronegative cell membranes, it was earlier for short chain PEI without crosslinked to fall off from MSN surface than the crosslinked PEI, resulting in more leakage of siRNA, during the entire process of internalization. The observation via confocal fluorescent microscopy as indicated in Fig. 4B was accordance with that of flow cytometry. Some punctate green fluorescence could be observed in the cytoplasm, suggesting that the nanoparticles had been internalized by cells.

In fact, to generate substantial gene silencing effect, it is not only necessary for siRNA to be transferred into the cells, but also escape from the endosome to work in the cellular cytoplasm. Thus, the intracellular distribution after trafficking into the cells and lysosome escape of siRNA was evaluated. KB cells were incubated with MSN-siRNA/CrPEI at 37°C for different incubation time (0.5 h, 1 h, 2 h, 3 h and 4 h) followed by live cell imaging under

a Leica SP5 confocal microscope. The endosome/lysosome was stained with Lysotracker Red. As shown in Fig. 4C, for FAM-siRNA loaded MSNs capped with crosslinked PEI (MSN-siRNA/CrPEI), the weak colocalization spots (yellow) of the green (FAM-siRNA) and red (Lysotracker Red) fluorescence could be found in the cytoplasm, indicating the majority of encapsulated siRNA was within endolysosomes in the early phase of uptake (0.5 h). However, as time went, the green fluorescence strengthened which suggested the uptake increased and partially separated from the red fluorescence over time (4 h), pointing the successful escape of FAM-siRNA and distribution in cytoplasm where siRNA mediated its function. This triggered rapidly escape is involved the proton sponge mechanism of PEI[20].

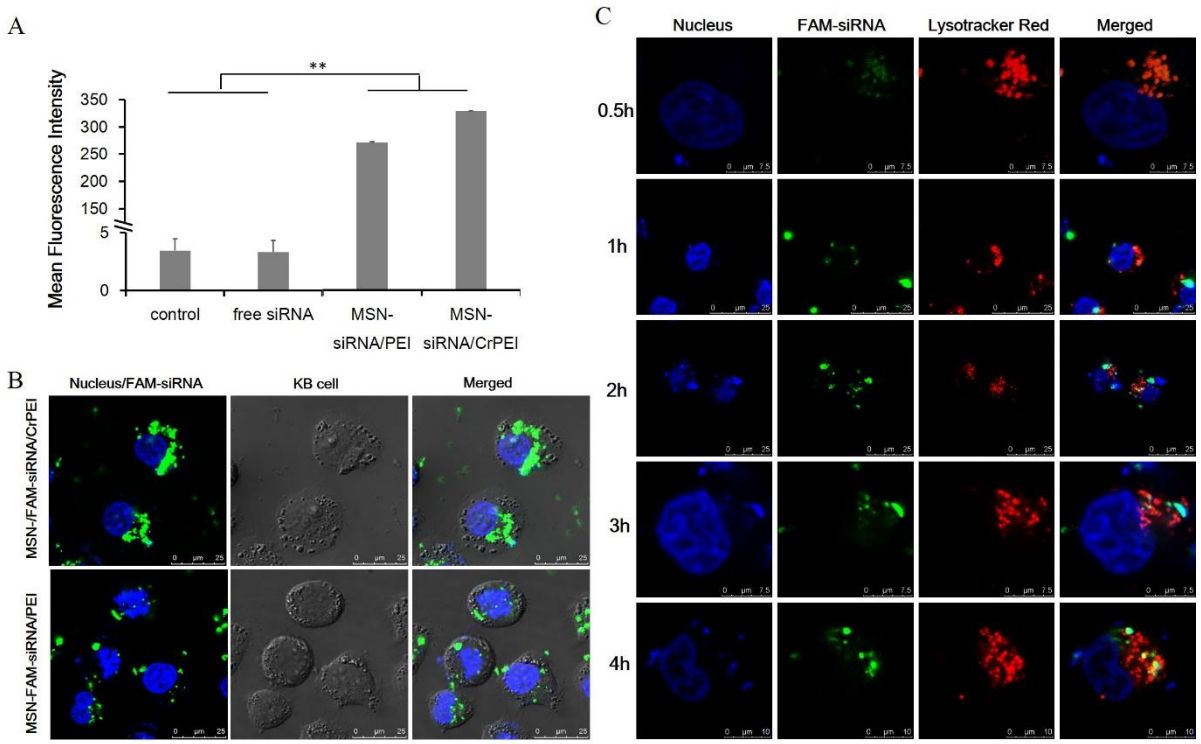

Fig. 4 Cellular uptake and intracellular trafficking of FAM-siRNA delivered by MSNs. (A) Fluorescence intensity of KB cells incubated with free siRNA, MSN-siRNA/PEI, MSN-siRNA/CrPEI at 37°C for 4 h as measured by flow cytometry. Cells treated with serum-free media were used as control. The data are expressed as the mean ± SD (n=3). **P<0.01. *P<0.05. (B) Intracellular trafficking of FAM-siRNA (50 nM) delivered by MSNs

incubated with KB cells and for 4 h. (C) Intracellular distribution of MSN-siRNA/CrPEI in KB cells after incubated for 0.5 h, 1 h, 2 h, 3 h and 4 h. Green, red and blue represent fluorescence of FAM-siRNA, Lysotracker red for endolysosomes and Hoechst 33258 for nuclei staining, respectively.

Effect of MSN-siRNA/CrPEI on cell activity

As we know, a critical issue for any nanocarrier application is nanoparticles' toxicity. Toxicity is associated with silanol groups on the surface of MSNs[11,36]. The cytotoxicity of MSN/CrPEI and bare MSNs was evaluated through the MTT assay. Fig. 5 showed the viability of KB cells incubated with MSNs for 48 h. It was found that MSN/CrPEI exhibited little toxicity to cells, even though the dose of MSNs reached as high as 100 μg/ml. While bare MSNs had toxic effects at high doses, since slight inhibition of cellular viability appeared at the dose of 100 μg/ml. A general consensus of toxicity from MSN is related to the silanol groups that can hydrogen bond to membrane or ionize to form SiO^- that lead to strong interaction and possibly membranolysis. What's more the silica surface present the reaction of radicals with water to yield reactive oxygen species (ROS) that also cause cell death[37]. In addition, the toxicity was associated with the cell line that MSNs performed different toxicity on different cell line. In our other study, the bare MSN showed no significant toxicity on MCF-7 cells (data not shown). Fortunately the toxicity can be decreased by surface modification to protect the exposed silanol groups[38].

It is known that PEI can induce the interaction with cell, which has toxicity especially at higher doses[39]. However, the previous study showed the corsslinked short chain PEI has a lower toxicity than the long chain[21] due to the lower positive charge, which may explain why the MSNs capping with corsslinked PEI didn't perform much toxicity. The results showed that the nanocarriers were highly compatible with cell membranes under physiological

conditions.

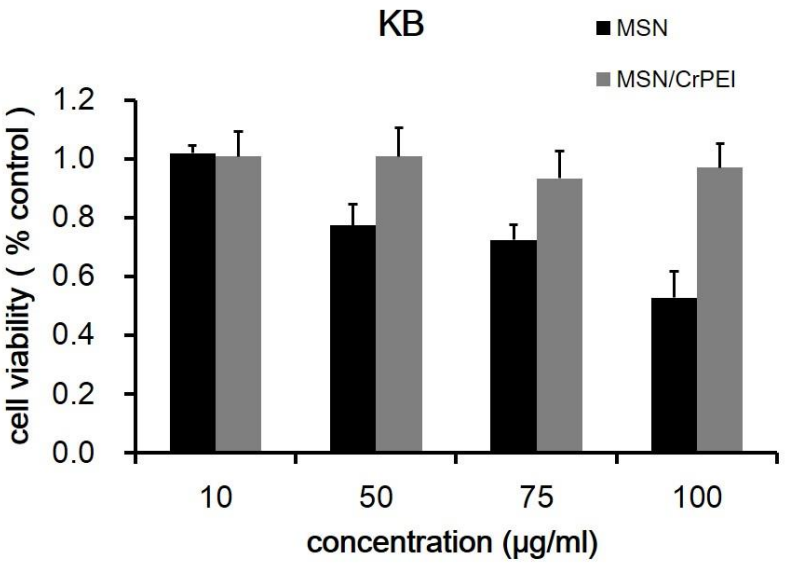

Fig. 5 The survival rate of KB cells cultured with bare MSNs and MSN/CrPEI for 48 h. Data are presented as the mean ± SD (n=5).

In vitro siRNA transfection and gene expression

We treated KB cells with loaded VEGF targeting siRNA MNSs and naked siRNA to verify gene suppression activity. As exhibited in Fig. 6A, compare with the control group, VEGF protein expression were significantly down-regulated in both MSN-siRNA/PEI (40%, $P<0.05$) and MSN-siRNA/CrPEI (75%, $P<0.01$). While the difference between the two preparation groups was thought for the better protective efficiency of the loading within MSN-siRNA/CrPEI than that of MSN-siRNA/PEI, resulting in a higher efficiency of siRNA delivery into cells, and better effect of target gene silencing.

To confirm that the suppression of VEGF expression indeed resulted from the VEGF RNA reduction mediated by VEGF siRNA in tumor cells, we adopt the method of qRT-PCR to detect the transcriptional VEGF mRNA level (Fig. 6B). Relative quantitative method of GAPDH being used as internal reference, is applied to calculate relative content of VEGF

mRNA. The results were consistent with that of VEGF protein expression. Treatment with MSN-siRNA/CrPEI caused a greater down-regulation of VEGF mRNA (~74%) compared with MSN-siRNA/PEI (~40%), whereas there was no apparent knockdown shown by naked VEGF siRNA and MSN-siN.C/CrPEI. The results were in accordance with the above assays of cellular uptake and endosomal escape, suggesting efficient delivery of bioactive siRNA into the cytosol.

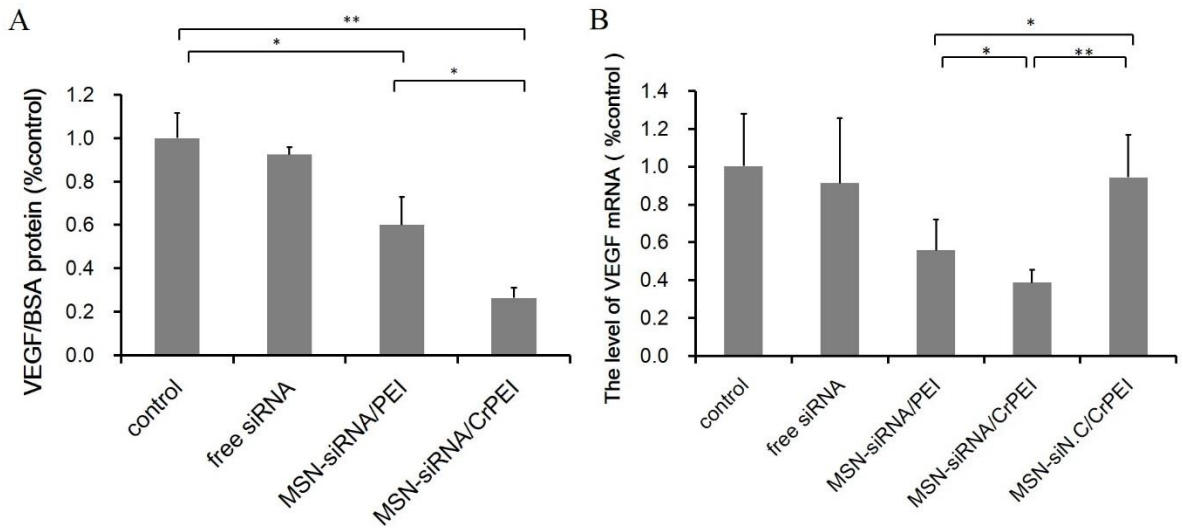

Fig. 6 (A) The level of VEGF protein/BSA protein and (B) VEGF mRNA expression determined by ELISA and quantitative real-time PCR after culturing with various formulations carrying VEGF siRNA in KB cells, respectively. KB cells were transfected with various samples carrying VEGF siRNA or siN.C at 37°C for 4 h. Data are presented as the mean ± SD (n=3). *P<0.05, **P<0.01.

In vivo tumor growth inhibition study

The MSN-siRNA/CrPEI had shown to be effective as expected in vitro. Therefore, the effect in vivo of nanoparticles loaded with siRNA was evaluated further to observe the therapeutic effect. Peritumoral administration of the MSN-siRNA/CrPEI (1.00 mg/kg VEGF siRNA) was performed on nude mice bearing a KB xenografted tumor, and compared with

control. As shown in Fig. 7, MSN-siRNA/CrPEI showed a higher inhibition of tumor growth (Fig. 7A) and smaller tumor size (Fig. 7B) and weight of excised tumors (Fig. 7C) compared with control group.

During the entire process of medication, body weight of both the control group and treatment group had a slight decline as shown in Fig. 7D, but there was no significant difference between two groups. The reason of weight loss should be that, the growth of tumor took in a large part of nutrition, and some factors secreted by tumor tissues would also cause the inflammatory response, thus having negative impact on mices' living situation.

To evaluate whether the reduced tumor growth was associated with VEGF gene silencing in vivo, VEGF expression at both the protein and mRNA levels within the tumor was determined. As shown in Fig. 7E and Fig. 7F, VEGF protein and mRNA levels of MSN-sRNA/CrPEI group was significantly inhibited about 46% ($P<0.05$) and 55% ($P<0.01$), respectively, compared with control.

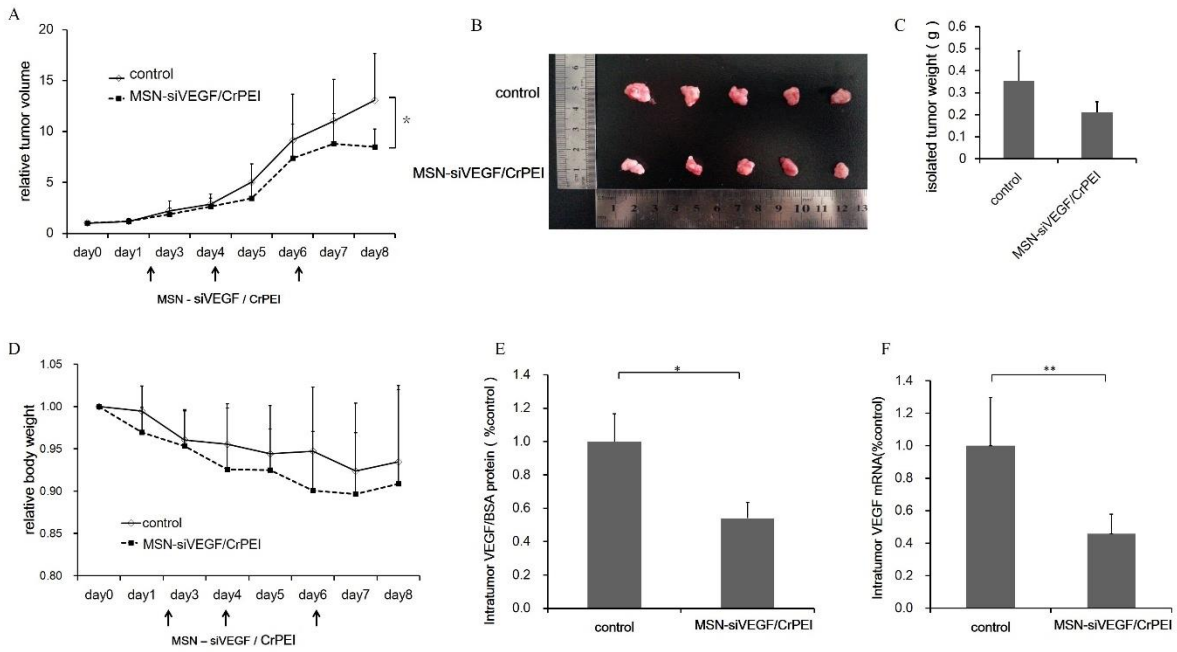

Fig. 7 (A) In vivo antitumor study of MSNs in KB tumor-bearing BALB/c nude mice after injected with 5% glucose (Control), MSN-siVEGF/CrPEI. The dose of siRNA was 1.00 mg/kg. Arrow represent the time of drug administration. Data are presented as the mean ± SD

(n=5-7). *P<0.05 as compared with controls. (B) Photograph and (C) the weights of the solid tumors removed from different treatment groups at the study termination. Data are presented as the mean ± SD (n=5). (D) The body weight variation of BALB/c nude mice implanted with KB cells after treatment. Data are presented as the mean ± SD (n=5). There were no significant differences (P > 0.05). (E) The expression level of intratumor VEGF protein and (B) mRNA in tumors. Data are presented as the mean ± SD (n=3). *P<0.05, **P<0.01.

MSN-siVEGF/CrPEI reduces interstitial fluid pressure, induce angiogenesis regression, and increases vascular perfusion in tumor

Normal tissues have an IFP close to 0 mm Hg, whereas an elevated IFP is found in experimental and human tumors[40,41], which is contributed by the absence of normal lymphatic system, the abnormally high permeability within the tumor vessels, and the increased propensity of microthrombus formation in both extravascular and vascular of tumor. The higher osmotic pressure is not conducive to the accumulation of antineoplastic drugs within the tumor tissue, thus the modification of interstitial hypertension is considered an important factor in antineoplastic therapy. MSN-siRNA/CrPEI treatment reduced IFP by 30% (Fig. 8A). The decrease indicated the medication could mediate tumor vascular normalization which improve the blood perfusion.

Immunofluorescent staining of tumor sections for the analysis of tumor vasculature and blood perfusion was performed. As indicated in Fig. 8B, control group had abundant CD31-positive tumor vessels and little blood flow. In contrast, a significantly reduction of the CD31-positive tumor vessels and enhancement of blood flow marked by fluorescent PSA were observed in VEGF siRNA treatment groups.

In tumor tissues, the physiological abnormalities associated with tumor vessels stimulates the overproduction of proangiogenic factors (i.e. VEGF)[42,43]. Proangiogenic factors promotes

the formation of new immature, tortuous, and hyperpermeable vessels[43], with messy endothelial cells, loosely attached pericytes, and aberrant distribution of vascular basement membrane[44,45]. These abnormalities lead to an impaired blood flow[46]. Precious literature[47] elucidated that the observed effect of anti-VEGF therapy in preclinical models is a result of both vascular regression and normalization. Vascular regression stand for the growth of immature vessels in the decline. The vascular normalization is characterized as vessel remodeling by the improvement of hyperpermeability, increased vascular pericyte coverage, more ordered basement membrane, and a reduction in tumor hypoxia and IFP and improved tumor vessel perfusion and oxygenation[45].

All of the results revealed that VEGF siRNA in the MSNs had delivered into tumor and made the effects, resulting in tumor vascular normalization, the increase of perfusion and the reduction of IFP, which linked to a reduction in tumor growth (Fig. 7).

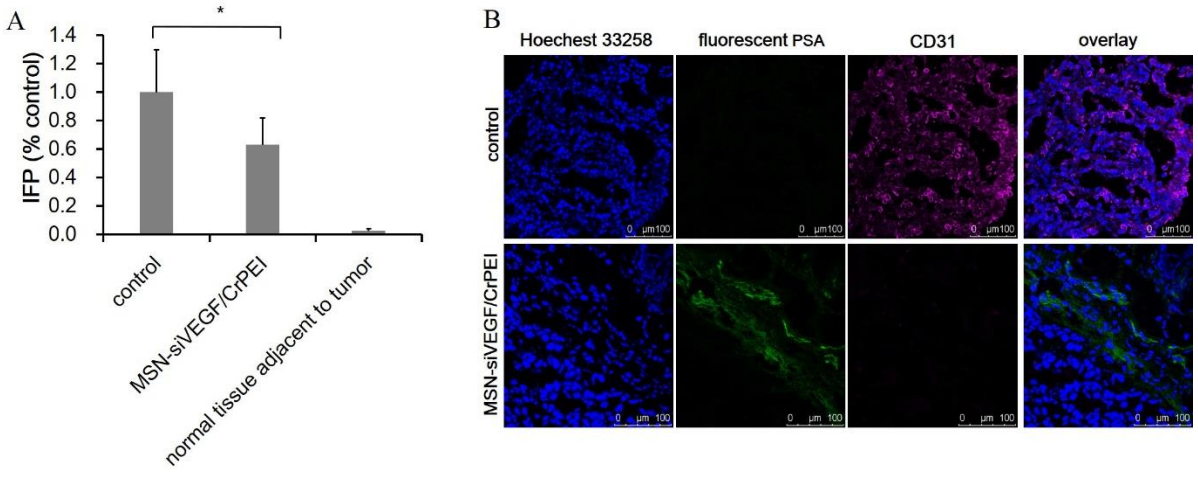

Fig. 8 (A) IFP in KB tumor-bearing BALB/c nude mice after injected with 5% glucose (Control) or MSN-siVEGF/CrPEI. The dose of siRNA was 1.00 mg/kg. Data are presented as the mean ± SD (n=4-5). *P<0.05 as compared with controls. (B) The immunohistochemistry of CD31 and fluorescent PSA represented vessels and perfusion.

siRNA combined with dexamethasone administration in vivo tumor growth inhibition

As we mentioned above, abnormalities associated vasculature in tumor contributes the high IFP, acting as the obstacle for delivery of macromolecules into solid tumors[40]. Lower IFP may be lead to an improvement in the delivery and efficacy of exogenously administered therapeutics. Dexamethasone (Dex), a glucocorticoid class steroid hormone, is widely used as a potent anti-inflammatory and bone growth steroid or chemotherapeutic drugs to treat childhood leukemia[48]. Dex had been also reported for its strong capability to decrease the IFP of mice bearing tumor[40]. So Dex was given into KB tumor-bearing BALB/c nude mice to determine whether combination of Dex and siRNA nanoparticles can improve the cancer therapy.

As shown in Fig. 9A, Dex group reduced IFP by almost 80% compared to control, indicating Dex has a strong capability to decrease the IFP. The combined administration groups (MSN-siRNA/CrPEI+Dex or MSN-siN.C/CrPEI+Dex) both showed lower IFP than MSN-siRNA/CrPEI group, indicating a stronger IFP reduction.

The result of immunofluorescent staining (Fig. 9B) suggested that most tumor cells of control group, Dex group and MSN-siN.C/CrPEI with Dex group had more expression of CD31, accounting for a large number of new blood vessels may distribute in tumor tissue. MSN-siRNA/CrPEI with Dex combined administration group had a lower vascular positive rate, showing VEGF siRNA played a role to inhibit the formation of tumor angiogenesis. Meanwhile, compared with the control group, siRNA treatment group had relatively high blood perfusion marked with fluorescent-PSA and a tendency to normal, which is consistent with the determination results of decreased IFP.

As a consequence of the lower IFP, combined administration showed the highest inhibition of tumor growth and smallest tumor size and weight of excised tumors compared with other groups (Fig. 9C and 9D). MSN-siVEGF/CrPEI group took the second place. Although applying Dex alone also showed a trend of inhibition of the tumor growth, no significant

difference with control, indicating siRNA is considered the dominated drug for the solid tumor therapy. During the entire process of medication, body weight of all the groups had a decline (Fig. 9E), especially for the Dex group. According to the literature[40], the dosage of Dex ranging from 0-30 mg/kg should be safe except the steroid toxicity which may cause a phenomenon that the tumors were eaten by the host animals or their peers. However during the process of experiment, we found the dosage of 3 mg/kg was high enough that it had induced the death of mice compared with the group received only siRNA.

VEGF protein expression and mRNA levels within the tumors were determined to evaluate if combined administration could make a greater effect on VEGF gene silencing in vivo. As shown in Fig. 9F, VEGF protein and mRNA levels of combined administration group and MSN-siRNA/CrPEI group didn't show much difference. The result also suggested siRNA should be the initiator who adjust the mRNA and protein expression and mediate the gene silencing.

Although the antitumor effects of combined administration of Dex and MSN-siRNA/CrPEI is the best, the distance to the ideal effect is still a big gap. A decreased IFP and improved perfusion may contribute the EPR effect[44], which provides a greater opportunity for more nanoparticles accumulated in the tumor. However, it is undeniable that long-term systemic exposure to Dex causes adverse side effects including slowed growth, stomach and intestinal bleeding causing by ulcers, damage to the joints, high blood sugar (Cushing's syndrome), high blood pressure (hypertension), and of the most importance, immunosuppression due to nonspecific killing of normal T and B lymphocytes[48]. So it is necessary to further study the treatment effects of Dex and balance the benefits and risks.

The VEGF-siRNA showed moderate anti-tumor efficacy and single VEGF inhibition could not completely suppress angiogenesis and tumor growth. Furthermore, the effect of siRNA is temporary[49]. But it is of the most importance that antiangiogenic, specifically anti-VEGF

therapy in tumors can normalize the vasculature that just can provide a window of opportunity for concurrent chemotherapy, which act as the main effect of cytotoxicity and collaborative work to generate the highest anti-tumor efficacy via multiple tumor inhibition pathways.

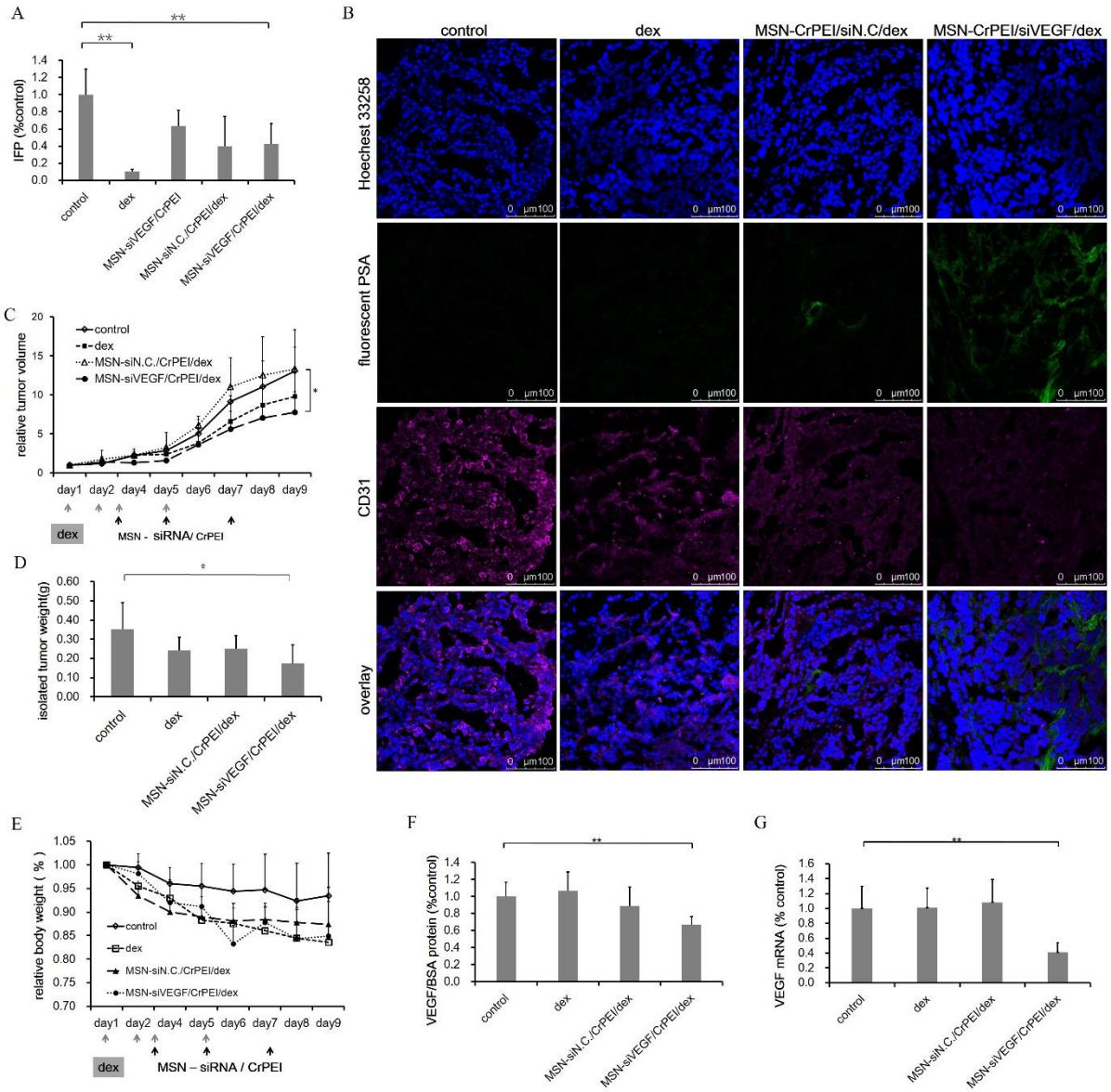

Fig. 9 Effects of dexamethasone combination with MSNs in KB tumor-bearing BALB/c nude mice. The dose of siRNA and Dex was 1.00 mg/kg and 3 mg/kg, respectively. (A) IFP. Data are presented as the mean ± SD (n=4 or 5), *P<0.05, **P<0.01 as compared with controls. (B) Immunohistochemisty of CD31 (red) and fluorescent PSA (green) represented vessels and

perfusion, respectively. (C) Relative tumor volumes. Arrow represent the time of drug administration. Data are presented as the mean ± SD (n=5-7). *P<0.05, **P<0.01 as compared with controls. (D) Weights of the removed tumors. Data are presented as the mean ± SD (n=5). *P<0.05, **P<0.01 as compared with controls. (E) Body weight variation of BALB/c nude mice implanted with KB cells after treatment. Data are presented as the mean ± SD (n=5-7). There were no significant differences (P>0.05). (F) The expression level of intratumor VEGF protein and (G) mRNA in tumors. Data are presented as the mean ± SD (n=3). *P<0.05, **P<0.01 as compared with controls.

Conclusion

In summary, we have successfully prepared MSNs capped with disulfide bond crosslinked PEI as nanoparticles to delivery siRNA. The MSN-siRNA/CrPEI possessed considerable siRNA loading capability, ascendant sensitivity to the reductive environment, negligible cytotoxicity to cells, readily internalization into cells and efficient escaping from the endolysosomes, so that the nanoparticles release the loaded siRNA molecules in cytoplasm, and mediate significant target gene silencing effect in tumor cells. As a result, the developed MSN-siRNA/CrPEI delivery system was able to facilitate anti-tumor efficacy, gene silencing and IFP reduction in KB xenografted tumors based on anti-angiogenesis and vascular normalization effects in vivo by targeting VEGF. In addition, the combined administration of the MSN-siRNA/CrPEI delivery system with dexamethasone exerted a better treatment effect which attributed to the strong ability of dexamethasone to decrease the IFP, and a lower IFP lead to an improvement in the delivery and efficacy of exogenously administered therapeutics. It is believed that the present MSN-siRNA/CrPEI delivery system can be further developed for effective strategy for siRNA delivery.

Acknowledgments

We would like to acknowledge National Key Basic Research Program (No. 2013CB932501), NSFC (No. 81273454, No. 81473156), Beijing NSF (No. 7132113), Doctoral Foundation of the Ministry of Education (No. 20130001110055) for funding of the work.

Reference:

1. D. Hanahan and J. Folkman, Cell, 1996, **86**, 353-364.
2. H. M. Verheul, H. Hammers, K. van Erp, Y. Wei, T. Sanni, B. Salumbides, D. Z. Qian, G. D. Yancopoulos and R. Pili, Clinical cancer research : an official journal of the American Association for Cancer Research, 2007, **13**, 4201-4208.
3. P. Carmeliet and R.K. Jain, Nature, 2000, **407**, 249-257.
4. C. G. Willett, Y. Boucher, E. di Tomaso, D. G. Duda, L.L. Munn, R. T. Tong, D. C. Chung, D. V. Sahani, S. P. Kalva, S. V. Kozin, M. Mino, K. S. Cohen, D. T. Scadden, A. C. Hartford, A. J. Fischman, J. W. Clark, D. P. Ryan, A. X. Zhu, L. S. Blaszkowsky, H. X. Chen, P. C. Shellito, G. Y. Lauwers and R. K. Jain, Nature medicine, 2004, **10**, pągs. 145-147.
5. A. R. Kirtane, S. M. Kalscheuer and J. Panyam, Advanced drug delivery reviews, 2013, **65**, 1731–1747.
6. N. S. Vasudev and A. R. Reynolds, Angiogenesis, 2014, **17**, 471-494.
7. L. Aagaard and J. J. Rossi, Advanced Drug Delivery Reviews, 2007, **59**, 75–86.
8. K. A. Whitehead, R. Langer and D. G. Anderson, Nature Reviews Drug Discovery, 2010, **8**, 129-138.

9. I. I. Slowing, J. L. Vivero-Escoto, C. W. Wu, and V. S. Y. Lin, Advanced drug delivery reviews, 2008, **60**, 1278–1288.
10. B. Liu, C. Li, P. Ma, Y. Chen, Y. Zhang, Z. Hou, S. Huang and J. Lin, Nanoscale, 2015, **7**, 1839-1848.
11. D. Tarn, C. E. Ashley, M. Xue, E. C. Carnes, J. I. Zink and C. J. Brinker, Acc Chem Res, 2013, **46**, 792-801.
12. P. Selvam, S. K. Bhatia and C. G. Sonwane, Ind. Eng. Chem. Res., 2001, **40**, 3237-3261.
13. H. Wen, J. Guo, B. Chang and W. Yang, Eur J Pharm Biopharm, 2013, **84**, 91-98.
14. M. Mizutani, Y. Yamada, T. Nakamura and K. Yano, Chemistry of materials, 2008, **20**, 4777-4782.
15. X. Li, Q. R. Xie, J. Zhang, W. Xia and H. Gu, Biomaterials, 2011, **32**, 9546–9556.
16. D. V. Svintradze and G. M. Mrevlishvili, Int J Biol Macromol, 2005, **37**, 283–286.
17. S. B. Hartono, W. Gu, F. Kleitz, J. Liu, L. He, A. P. J. Middelberg, C. Yu, G. Q. Lu and S. Z. Qiao, ACS Nano, 2012, **6**, 2104-2117.
18. P. Horcajada, A. Rámila, J. Pérez-Pariente and M. Vallet-Regı, Microporous and Mesoporous Materials, 2004, **68**, 105–109.
19. Z. Z. Yang, J. Q. Li, Z. Z. Wang, D. W. Dong and X. R. Qi, Biomaterials, 2014, **35**, 5226–5239.
20. A. Akinc, M. Thomas, A. M. Klibanov and R. Langer, J Gene Med, 2005, **7**, 657–663.
21. R. Deng, Y. Yue, F. Jin, Y. Chen, H. F. Kung, M. C. M. Lin and C. Wu, Journal of Controlled Release, 2009, **140**, 40–46.
22. E. Fleige, M. A. Quadir and R. Haag, Advanced drug delivery reviews, 2012, **64**, 866–

884.

23. G. Saito, J. A. Swanson and K. D. Lee, Advanced drug delivery reviews, 2003, **55**, 199–215.

24. G. Wu, Y. Z. Fang, S. Yang, J. R. Lupton and N. D. Turner, Journal of Nutrition, 2004, **134**, 489-492.

25. F. Meng, W. E. Hennink and Z. Zhong, Biomaterials, 2009, **30**, 2180–2198.

26. M. H. Kim, H. K. Na, Y. K. Kim, S. R. Ryoo, H. S. Cho, K. E. Lee, H. Jeon, R. Ryoo and D. H. Min, ACS nano, 2011, **5**, 3568-3576.

27. M. Neu, O. Germershaus, S. Mao, K. H. Voigt, M. Behe and T. Kissel, Journal of Controlled Release, 2007, **118**, 370–380.

28. W. Gao, B. Xiang, T. T. Meng, F. Liu and X. R. Qi, Biomaterials, 2013, **34**, 4137-4149.

29. M. Kato, Y. Hattori, M. Kubo and Y. Maitani, International journal of pharmaceutics, 2012, **423**, 428–434.

30. M. Murakami, M. J. Ernsting, E. Undzys, N. Holwell, W. D. Foltz and S. D. Li, Cancer research, 2013, **73**, 4862-4871.

31. X. Li, J. Zhang and H. Gu, Langmuir, 2011, **27**, 6099-6106.

32. P. Chomczynski and N. Sacchi, Nature Protocols, 2006, **1**, 581-585.

33. X. Li, Y. Chen, M. Wang, Y. Ma, W. Xia and H. Gu, Biomaterials, 2013, **34**, 1391–1401.

34. S. Aluri, S. M. Janib and J. A. Mackay, Advanced Drug Delivery Reviews, 2009, **61**, 940–952.

35. R. K. Jain and T. Stylianopoulos, Nature reviews. Clinical oncology, 2010, **7**, 653-664.

36. I. I. Slowing, C. W. Wu, J. L. Vivero-Escoto and V. S.Y. Lin, Small, 2009, **5**, 57–62.

37. M. A. A. Schoonen, C. A. Cohn, E. Roemer, R. Laffers, S. R. Simon and T. O'Riordan, Reviews in Mineralogy and Geochemistry, 2006, **64**, 179-221.

38. D. Tarn, C. E. Ashley, M. Xue, E. C. Carnes, J. I. Zink and C. J. Brinker, Accounts of chemical research, 2013, **46**, 792-801.

39. J. Hoon Jeong, L. V. Christensen, J. W. Yockman, Z. Zhong, J. F. Engbersen, W. Jong Kim, J. Feijen and S. Wan Kim, Biomaterials, 2007, **28**, 1912–1917.

40. P. E. Kristjansen, Y. Boucher and R. K. Jain, Cancer research, 1993, **53**, 4764-4766.

41. Y. Boucher and R. K. Jain, Cancer research, 1992, **52**, 5110-5114.

42. M. Datta, L. E. Via, W. S. Kamoun, C. Liu, W. Chen, G. Seano, D. M. Weiner, D. Schimel, K. England, J. D. Martin, X. Gao, L. Xu, C.E. Barry and R. K. Jain, Proceedings of the National Academy of Sciences of the United States of America, 2015, **112**, 1827-1832.

43. P. Carmeliet and R. K. Jain, Nature Reviews Drug Discovery, 2011, **10**, 417-427.

44. N. Bertrand, J. Wu, X. Xu, N. Kamaly and O. C. Farokhzad, Advanced drug delivery reviews, 2014, **66**, 2-25.

45. P. Baluk, H. Hashizume and D. M. McDonald, Current opinion in genetics & development, 2005, **15**, 102–111.

46. R. K. Jain, Journal of Clinical Oncology : Official Journal of the American Society of Clinical Oncology, 2013, **31**, 2205-18.

47. S. Goel, D. G. Duda, L. Xu, L. L. Munn, Y. Boucher, D. Fukumura and R. K. Jain, Physiological Reviews, 2011, **91**, 1071-1121.

48. V. Krishnan, X. Xu, S. P. Barwe, X. Yang, K. Czymmek, S. A. Waldman, R. W. Mason,

X. Jia and A. K. Rajasekaran, Molecular Pharmaceutics, 2012, **10**, 2199-2210.

49. Z. X. Lu, L. T. Liu and X. R. Qi, International Journal of Nanomedicine, 2011, **6**, 1661-1673.